Cement & Concrete Composites 42 (2013) 30–40

Contents lists available at SciVerse ScienceDirect

Cement & Concrete Composites

journal homepage: www.elsevier.com/locate/cemconcomp

Lattice modeling of chloride diffusion in sound and cracked concrete

Branko Šavija *, José Pacheco, Erik Schlangen

Delft University of Technology, Stevinweg 1, 2628 CN Delft, The Netherlands

ARTICLE INFO

Article history:
Received 25 August 2012
Received in revised form 9 May 2013
Accepted 13 May 2013
Available online 23 May 2013

Keywords:
Lattice model
Mesoscale
Cracking
Chloride diffusion
Durability

ABSTRACT

Reinforced concrete structures are frequently exposed to aggressive environmental conditions. Most notably, chloride ions from sea water or de-icing salts are potentially harmful since they promote corrosion of steel reinforcement. Concrete cover of sufficient quality and depth can ensure protection of the steel reinforcement. However, it is necessary to study the effects of material heterogeneity and cracking on chloride ingress in concrete. This is done herein by proposing a three-dimensional lattice model capable of simulating chloride transport in saturated sound and cracked concrete. Means of computationally determining transport properties of individual phases in heterogeneous concrete (aggregate, mortar, and interface), knowing the concrete composition and its averaged transport properties, are presented and discussed. Based on numerical experimentation and available literature, a relation between the effective diffusion coefficient of cracked lattice elements and the crack width was adopted. The proposed model is coupled with a lattice fracture model to enable simulation of chloride ingress in cracked concrete. The model was validated on data from the literature, showing good agreement with experimental results.

1. Introduction

Modern reinforced concrete structures, if properly designed and executed, can achieve their intended service life. Corrosion of reinforcing steel due to chloride ingress can be prevented. An increasing number of service life models are available to aid the practicing engineer. These are all based on one, but very crucial, assumption: that the structure in question is and remains crack free. Evidently, this is almost never the case: reinforced concrete structures crack due to many reasons, most important ones being mechanical loading and shrinkage. This has been an issue of increasing focus in the research community lately: a number of publications deals with experimental investigations on the influence of cracking on chloride ingress (see [1]) and reinforcement corrosion (see [2]) in cracked concrete.

Apart from experimental studies on the subject, a number of models have been proposed in the literature. Some of them model the effect of cracking in a smeared way, by introducing an increase of the diffusion coefficient in the whole domain (e.g. [3]). Others model cracks as notches or faults in concrete, without the mechanical analysis (e.g. [4,5]). Very few have made a step further, and coupled the mechanical and transport analyses (e.g. [6]). Most of these models treat concrete as a quasi-homogeneous continuum, i.e. mechanical and transport properties are constant for the whole domain. On the other hand, a truss-network approach proposed by Wang and Ueda [7], considers concrete as a three-phase composite, consisting of coarse aggregate, mortar, and ITZ. Both of these approaches (homogeneous and heterogeneous) are applicable within the lattice framework as presented here.

In the following, a three dimensional lattice model for simulating chloride penetration in sound and cracked concrete is presented. Governing equations and discretization procedure are addressed. The focus of the paper lies on determination of transport properties of different phases in concrete (aggregate, mortar, and the interface), and cracks. The model is validated using experimental results from the literature. Finally, these results are discussed and evaluated, and some conclusions are drawn.

2. Method

2.1. Chloride transport in concrete

Different physical and chemical transport mechanisms can contribute to chloride ingress, and they depend on the concrete pore structure, (micro) environmental conditions, temperature, moisture content in concrete, etc. Cracking of the concrete cover, due to e.g. loading or shrinkage, can alter the (local) mechanism of chloride ingress significantly. The transport mechanisms of chloride are usually categorized in four groups [8]:

* Corresponding author. Tel.: +31 (0)15 27 88986; fax: +31 (0)15 27 86383.
E-mail addresses: b.savija@tudelft.nl (B. Šavija), j.pachecofarias@tudelft.nl (J. Pacheco), h.e.j.g.schlangen@tudelft.nl (E. Schlangen).

0958-9465/$ - see front matter © 2013 Elsevier Ltd. All rights reserved.
http://dx.doi.org/10.1016/j.cemconcomp.2013.05.003

- *Diffusion*, where the transport of chloride is driven by concentration difference of chloride in various zones. The chloride diffuses in the pore solution of concrete from the zones of higher concentration to zones with lower concentration of chloride.
- *Permeation*, where the transport of chloride ions is driven by a difference of hydraulic pressure in various zones.
- *Migration*, where the transport of chloride ions is driven by a difference in electrical potential. Chloride ions always migrate into zones with lower electrical potential.
- *Convection* or *capillary suction*, where the chloride transport is driven by a difference in moisture content (pressure). In dry or partly dry concrete, water containing chloride moves towards zones with lower moisture content due to surface tension acting in the capillaries.

In general, any of these mechanisms, or a combination of them, can govern the ingress of chloride ions into concrete.

The degree of pore saturation is an important parameter influencing ionic transport in concrete; the diffusion process is most effective when the concrete is fully water saturated, although it can also take place in partially saturated concrete. It can be considered that chloride diffusion is the governing transport mechanism when concrete is fully saturated; in a partially saturated condition, chlorides are transported by means of several combined mechanisms.

Transport of chloride ions in non-saturated sound concrete is a complicated issue and is still an important topic of research. Therefore, in order to simplify studies of chloride ingress in cracked concrete, laboratory specimens are usually water saturated. For all analyses performed in this paper, the concrete pore system is assumed to be fully saturated with water. Under this assumption, ionic diffusion is considered to be the sole mechanism governing the transport of chloride ions.

2.2. Model description

Lattice models have long been used in fracture mechanics of concrete [9]. Recently, the use of lattice (or rather discrete) models has been extended on simulating transport processes in concrete [7,10–14]. Coupling of the mechanical and transport simulations, while taking into account the effect of cracking on the transport mechanism, was performed by [11–14]. In the mechanical lattice approach, concrete is discretized as a set of truss or beam elements. In the transport lattice approach, concrete is treated as an assembly of one-dimensional "pipes", through which the flow takes place. While some authors use "dual" lattices (one for the mechanical simulation, and the other for the flow simulation – for details see [12–14]) the approach proposed here uses the same lattice network for both simulations. In this approach, mechanical simulation is performed first; its output is then used as an input for simulating chloride ingress. Therefore, it is actually a one-way coupling – mechanical degradation does effect the chloride penetration, while, on the other hand, there is no influence of the chloride penetration on the mechanical behavior.

2.2.1. Spatial discretization

For the spatial discretization of the specimen in three dimensions, the basis is the prismatic domain. Discretization of the domain is performed according to the following procedure: first, the domain is divided into a number of cubic cells. As an input value, number of cells in x, y and z direction, and cell size, are specified. Then, a network of cubic cells is generated, and a sub-cell can be defined within each cell. A node is randomly placed in every sub-cell using a (pseudo) random number generator (Fig. 1).

Voronoi tessellation of the prismatic domain with respect to the specified set of nodes is performed. Nodes with adjacent Voronoi cells are connected by lattice elements (Fig. 2). Since Voronoi diagrams are dual with Delaunay tessellation, this approach is equivalent to performing a Delaunay tessellation of the set of nodes, as outlined by Yip et al. [15].

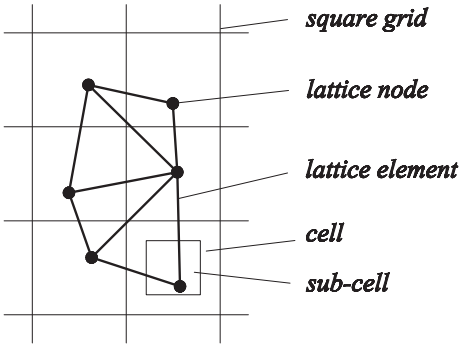

Fig. 1. Two-dimensional node-placement procedure.

The length ratio of the sub-cell to the cell defines the degree of randomness of the lattice. The degree of randomness can be between 0 and 1. When it is 0, the node is placed at the center of each cell. When it is 1, the sub-cell is identical to the cell. However, there is a small probability then that two nodes of neighboring cells are identical. Consequently, it is advised to use a value smaller than 1. In all presented simulations, the degree of randomness was set to 0.99.

In order to take material heterogeneity into account, the particle overlay procedure (schematically shown in Fig. 3) is employed: it is in this manner that different transport (or mechanical) properties are assigned to different phases. For this purpose, either a computer-generated material structure [16], or a material structure obtained by micro-CT scanning [17,18] can be used. Each node is assigned a voxel from the used microstructure. Element properties depend on the voxel value of its end nodes (see Fig. 3). What has to be noted here is that interface, as used in the present model, does not exactly coincide with the interfacial transition zone (ITZ). Its thickness is between 30 and 80 μm [19], while on the other hand interface elements in the present model take up also a piece of aggregate and a piece of mortar (Fig. 3). Their actual size in the model depends on the characteristic element size (voxel size).

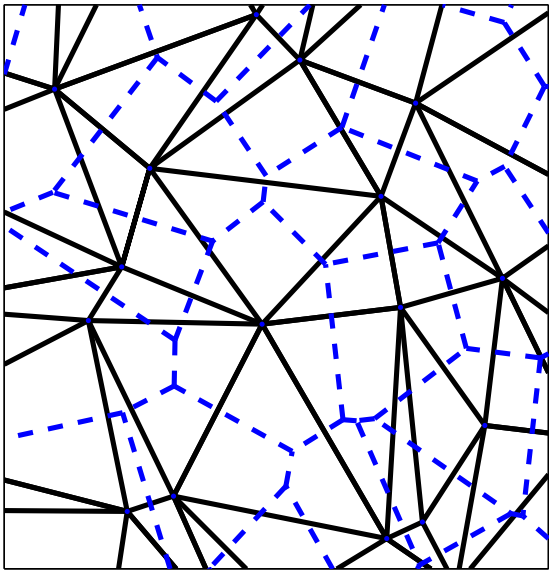

Fig. 2. Two-dimensional meshing procedure. Solid – lattice mesh; dashed – Voronoi tessellation.

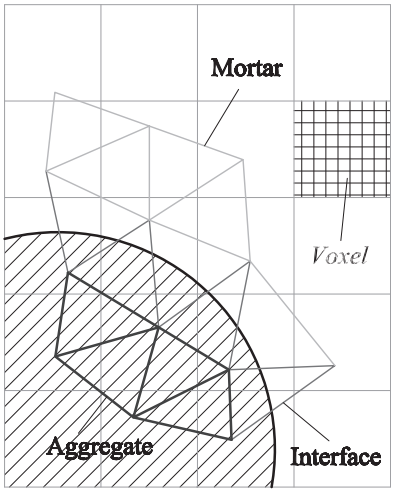

Fig. 3. Two-dimensional particle overlay procedure.

Therefore, the transport properties of this "phase" are slightly altered, as explained later.

It is important to note that, in general, nodes are not placed on the boundary of the analyzed domain (see Fig. 2). This creates some error in the boundary-condition application. Due to the relatively small voxel size usually used in the simulation, generally it can be discarded.

2.2.2. Mechanical model

In the model, continuum is discretized as an assembly of beam elements [11,20]. All elements are linear elastic. When loading is applied, a crack is formed by removing the element which has the highest stress/strength ratio and this ratio is greater than unity. These steps are repeated until the system fails, or a pre-described value of load has been reached. Realistic cracking patterns are achieved. The model has been successfully used in fracture modeling of mortar, concrete, and fiber-reinforced concrete. Details on the underlying equations for the 3D analysis, element matrices, and implementation can be found in [17]. Here, the focus is on the coupling of the available mechanical model with the chloride diffusion model.

2.2.3. Chloride diffusion model

The proposed model treats concrete as an assembly of one-dimensional "pipe" elements, through which chloride diffusion takes place. An assembly of these elements in 3 spatial dimensions enables the simulation of chloride penetration in 3D. As stated, chloride diffusion is assumed to be the only parameter governing chloride transport. The scope of the current study is, therefore, limited to water saturated conditions only.

The governing equation for the chloride diffusion simulation is Fick's second law [8]:

$$\frac{\partial C}{\partial t} = D\frac{\partial^2 C}{\partial x^2} \tag{1}$$

for the whole domain, Ω. Here, C is the chloride content, D the chloride diffusion coefficient, and x the spatial coordinate. The boundary conditions for this type of problem are [21]:

$$C = C_b \qquad \text{on } \Gamma_b \tag{2}$$

$$q = -D\frac{\partial C}{\partial n} \qquad \text{on } \Gamma_q \tag{3}$$

where $\Gamma_b \cup \Gamma_q = \Gamma$ and $\Gamma_b \cap \Gamma_q = 0$ is the whole boundary of the domain. In the above equation, q is outward flux normal to the boundary (i.e. in direction n), and C_b is the prescribed chloride content at the boundary. The initial condition for the problem is:

$$C = C_0 \quad \text{at } t = 0 \tag{4}$$

The chloride content is discretized in space as:

$$C(x,t) = \sum_{i=1}^{n} N_i C_i(t) \tag{5}$$

where N_i are the shape functions, n the number of nodes in an element, and $C_i(t)$ the time dependent nodal chloride contents. The Galerkin approximation of Eq. (1) is [21]:

$$\int_\Omega Ni\left(\frac{\partial}{\partial x}D\frac{\partial C}{\partial x} - \frac{\partial C}{\partial t}\right)d\Omega = 0 \tag{6}$$

Employing integration by parts on the first term of Eq. (6) yields:

$$-\int_\Omega \left(D\frac{\partial N_i}{\partial x}\frac{\partial C}{\partial x} + \frac{\partial C}{\partial t}\right)d\Omega + \int_{\Gamma_q} N_i D\frac{\partial C}{\partial x}nd\Gamma_q = 0 \tag{7}$$

From Eq. (3) it holds:

$$\int_{\Gamma_q} N_i D\frac{\partial C}{\partial x}nd\Gamma_q = -\int_{\Gamma_q} N_i q d\Gamma_q \tag{8}$$

On substituting the spatial discretization from Eqs. (5) and (7) becomes:

$$-\int_\Omega \left(D\frac{\partial N_i \partial N_j}{\partial x\ \partial x}C\right)d\Omega + \int_\Omega N_i N_j \frac{\partial C}{\partial t}d\Omega - \int_{\Gamma_q} N_i q d\Gamma_q = 0 \tag{9}$$

or, in matrix form:

$$M\frac{\partial C}{\partial t} + KC = f \tag{10}$$

Here M is the element mass matrix, K the element diffusion matrix, and f the forcing vector. For one-dimensional linear elements, as used here, the shape functions (N_i, N_j) and their derivatives (B_i, B_j) are [21]:

$$\begin{bmatrix} N_i \\ N_j \end{bmatrix} = \begin{bmatrix} 1 - \frac{x}{l} \\ \frac{x}{l} \end{bmatrix}$$

$$\begin{bmatrix} B_i \\ B_j \end{bmatrix} = \begin{bmatrix} \frac{\partial N_i}{\partial x} \\ \frac{\partial N_j}{\partial x} \end{bmatrix} = \begin{bmatrix} -\frac{1}{l} \\ \frac{1}{l} \end{bmatrix}$$

The relevant elemental matrices (Eq. (10)) for a one-dimensional element are:

$$K = \int_\Omega B^T D B d\Omega = DA\int_l B^T B dx = \frac{DA}{l}\begin{bmatrix} 1 & -1 \\ -1 & 1 \end{bmatrix}$$

$$M = \frac{1}{\omega}\int_\Omega N^T N d\Omega = \frac{A}{\omega}\int_l N^T N dx = \frac{Al}{6\omega}\begin{bmatrix} 2 & 1 \\ 1 & 2 \end{bmatrix}$$

$$f = -\int_{\Gamma_q} q N^T d\Gamma_q = \begin{bmatrix} -q_i A \\ -q_j A \end{bmatrix}$$

Note that $d\Omega$ in Eqs. (13) and (14) is replaced by Adx. Here, A is the uniform cross-sectional area of a one-dimensional element. Further, l and D are the length and the diffusion coefficient of each element, respectively. In Eq. (15) q_i and q_j are the prescribed nodal fluxes at nodes i and j. Cross sectional areas of individual elements are assigned using the so-called Voronoi scaling method [11] – cross section of an element is equal to the area of a facet of a Voronoi cell which is common to its end nodes (see Section 2.2.1). Ele-

ment mass and diffusion matrices (Eqs. (13) and (14)) are the same as those of regular one-dimensional linear elements [21], except the correction parameter ω in the mass matrix (Eq. (14)). This parameter is added to convert the volume of a Voronoi cell to the volume of lattice elements, due to overlap volume of adjacent lattice elements (Fig. 4):

It can be determined as [14]:

$$\omega = \frac{\sum_{k=1}^{m} A_k \cdot l_k}{V} \tag{16}$$

where n is the total number of elements, A_k and l_k cross sectional area and length of each lattice element, k element number, and V the volume of the specimen. It was shown that ω can be set as 2 for a two-dimensional and 3 for three-dimensional cases, respectively, without loss of accuracy [11,14]. Using the Crank–Nicholson procedure [21], the system of linear Eq. (10) is discretized in time, and the following equation results (when no flux boundary conditions are applied, i.e. f=0):

$$\left(M + \frac{1}{2}\Delta t \cdot K\right) C^n = \left(M - \frac{1}{2}\Delta t \cdot K\right) C^{n-1} \tag{17}$$

This equation is then solved for each discrete time step (Δt) and chloride profiles are obtained.

Saturated concrete was assumed in all analyses, since the purpose of this work was to validate the approach by comparing the results with experimental data, not to develop a fully functional service-life modeling tool. Therefore, Fick's second law (Eq. (1)) was assumed to be valid, and diffusion was the only transport mechanism considered.

For elements which are cracked, D in the diffusion matrix (Eq. (13)) is replaced by D_{CR}, an effective diffusion coefficient dependent on the local element crack width. Dependence of D_{CR} on the element crack width is elaborated in Section 2.4.

2.3. Phase transport properties

In order to determine transport properties of individual phases within the heterogeneous concrete, the approach developed by Caré and Hervé [22] (the so-called n-phase model) was used. This analytical model takes into account the characteristics of different phases of concrete on the effective diffusion coefficient of the composite material. The material is treated as a three-phase composite, consisting of a mortar phase, aggregate phase, and an interface transition phase. This model considers an n-layered spherical inclusion embedded in a matrix. In case of concrete, the aforementioned three phases are distinguished. Hence, the model assumes that, at mesoscopic scale, the effective diffusion coefficient of concrete (D_{eff}) is a function of the volume fraction and the diffusion coefficient of different phases (here: aggregate, mortar, and interface phase). This model was developed with spherical particles in mind, so for any other particle shape (e.g. the Anm material model developed by Qian [16]) can be considered as only an approximation. The following formulae were used (assuming impermeable aggregates):

$$D_{eff}/D_M = N/D \tag{18}$$

Here, the following are:

$$N = 6D_M(1 - C_A)(C_A + C_I) + 2C_I(D_I - D_M)(1 + 2C_A + 2C_I)$$
$$D = 3D_M(2 + C_A)(C_A + C_I) + 2C_I(1 - C_A - C_I)(D_I - D_M)$$

Here, D_M, and D_I are the diffusion coefficient of the mortar phase, and the diffusion coefficient of the interface phase, respectively. Also, C_A and C_I are volume fractions of the aggregate and the interface phases, respectively. If the aggregates are porous (e.g. calcareous aggregates), a different set of formulae, which take the diffusivity of the aggregate particles into account, can be used [22]. This approach enables one to determine the diffusion coefficient of individual phases (mortar and interface) in concrete, given the volumetric contents of each phase, and the effective diffusion coefficient of concrete. All these are usually available from the experimental data. Therefore, in order to determine this, it is necessary to determine the ratio between the diffusion coefficient of mortar and the diffusion coefficient of the interface.

To estimate the magnitude of this relation, a set of experimental data provided by Oh and Jang [23] was used (Table 1). Here, transport properties of concrete are compared to corresponding mortars. Concrete used in the experiments contained about 35% coarse aggregate by volume. Rapid chloride migration test was used in order to determine the non-steady state migration coefficient (D_{NSSM}) of concretes and mortars. From these, diffusion coefficients (D) were calculated.

By careful observation of the results (Table 1), it is clear that the ratio of mortar to concrete diffusion coefficient (M/C) changes dramatically when the diffusion coefficients are calculated. It even states that, in some cases, the diffusion coefficient of mortar is higher than that of concrete, even though its non-steady state migration coefficient is lower. This is hardly to be the case. In order to correct this, diffusion coefficients of concrete were calculated using a suggestion from [24]: it is stated that there exists a linear relationship between the non-steady state migration coefficient (D_{NSSM}) and the diffusion coefficient of concrete (D). Similarly, Yang and Wang [25] found that there is a linear relationship between

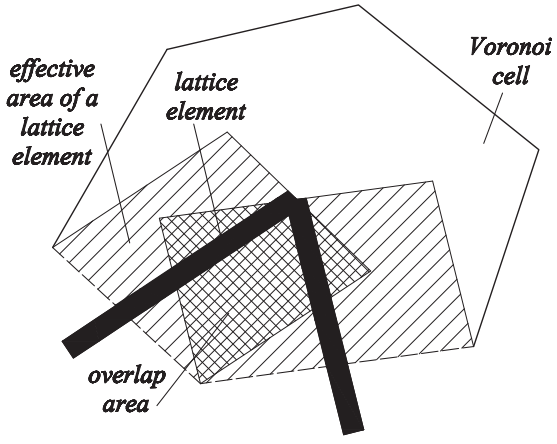

Fig. 4. Definition of overlap area for determination of parameter ω (adapted from [14]).

Table 1
Experimental results of [23] (C – concrete, M – mortar).

ID[a]	D_{NSSM} ($\times 10^{-12}$ m^2/s)			D ($\times 10^{-12}$ m^2/s)		
	C	M	M/C[b]	C	M	M/C[b]
NI-0	6.56	8.80	1.34	2.43	5.53	2.28
NI-PFA15	3.54	4.55	1.29	1.47	3.18	2.17
NI-BFS15	5.77	6.79	1.18	2.16	4.31	2.00
NI-BFS30	5.42	4.93	0.91	2.00	3.09	1.54
NV-0	9.43	11.94	1.27	3.35	7.20	2.15
NV-PFA30	3.43	5.04	1.47	1.19	2.94	2.47
NV-BFS30	4.68	5.49	1.17	1.70	3.39	2.00
LI-0	15.7	11.23	0.71	5.48	6.64	1.21
HI-0	3.76	5.4	1.44	1.49	3.56	2.40
HI-BFS30	3.54	2.92	0.82	1.42	1.96	1.37

[a] Different concrete/mortar mix designs from [23].
[b] Not provided in [23].

Table 2
Calculated diffusion coefficients.

ID	D ($\times 10^{-12}$ m^2/s)		
	C	M	D_I/D_M
NI-0	3.70	4.97	2.79
NI-PFA15	0.78	1.01	3.06
NI-BFS15	2.94	3.46	3.57
NI-BFS30	2.60	2.36	5.23
NV-0	6.48	8.21	3.14
NV-PFA30	0.68	1.00	2.24
NV-BFS30	1.88	2.21	2.46
LI-0	12.56	8.98	7.16
HI-0	1.00	1.44	2.39
HI-BFS30	0.78	0.65	5.94

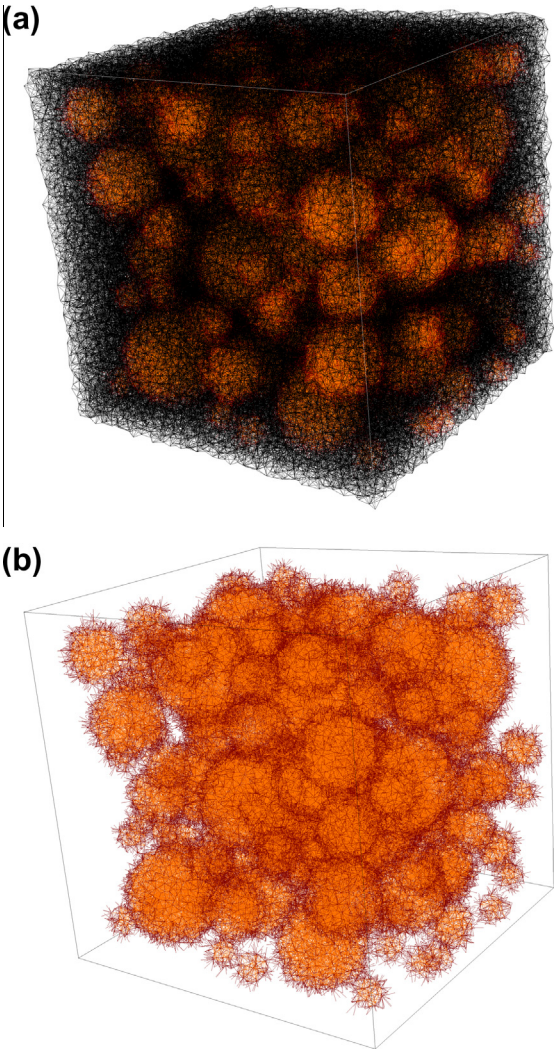

Fig. 5. (a and b) Determination of the D_I/D_M ratio (top-the whole lattice; bottom-only aggregate and the interface).

the non-steady state diffusion coefficient obtained from the accelerated chloride migration test (ACMT), and the diffusion coefficient obtained from the ponding test, irrespective of the concrete composition. Linear regression of the data provided by [24] yields the following tentative equation:

$$D = 0.97D_{NSSM} - 2.64 \quad (20)$$

where D and D_{NSSM} are in 10^{-12} m^2/s. Furthermore, by employing the M/C ratio from the migration experiment, the diffusion coefficient of mortar is calculated (Table 2). It has to be noted that Eq. (20) is used here merely as a tool to calculate the diffusion coefficient from the non-steady state migration coefficient.

In order to determine the ratio between the diffusion coefficient of mortar and the diffusion coefficient of the interface (D_I/D_M ratio), a concrete material structure with about 35% of coarse (spherical) aggregates was generated using a simple packing algorithm. Diameters of the coarse aggregate particles were in range of 4–24 mm. A lattice with characteristic elements size (voxel size) of 1 mm was projected on top of it, and volume of lattice elements of each phase was calculated (58.41% mortar, 29.35% aggregate, and 12.24% interface). Then, using formulae (18) and (19), the ratio between the diffusion coefficient of mortar and the diffusion coefficient of the interface was calculated for each mixture (Table 2). In order to achieve the desired effective concrete properties, these vary in the range 2.24–7.16. This seems to be in accordance with the variability of the diffusion coefficient of ITZ, which is stated to be somewhere in the range 2–8 times that of the cement paste [19].

The variability of this parameter can also be taken into account in a statistical manner; however more experimental results are needed to justify this approach. Based on presented analysis, a deterministic value of 3 for the D_I/D_M ratio was selected. This value is used in further analyses (see Fig. 5).

2.4. Crack transport properties

Two sets of experiments performed by Ismail et al. [26,27] are used for determining transport properties of a single crack. They used the expansive core method to create parallel-walled cracks in doughnut shaped specimens. Due to a large variety of smaller crack widths, these experiments are suitable for the procedure employed here. First set of experiments [26] was performed on cracked brick samples, while the second set [27] used cracked mortar samples. In both instances, cracked samples were placed in a chloride penetration cell, with chloride loading on both sides of the sample. After the exposure period, using the grinding technique, two types of chloride profiles were determined: perpendicular to the exposed surface, and perpendicular to the crack walls. The second type of profiles were determined by grinding the material in the middle part of the specimen height, in order to ensure that powder samples would contain only chloride ions penetrating from the crack plane, and not from the sample surface (Fig. 6).

Here, the approach proposed by Wang and Ueda [7] was used. In order to determine the effective crack transport properties, numerical simulation results are fitted to experimental data. For the simulations, the geometry of the test (Fig. 6) was simplified: a prismatic 3D lattice of $50 \times 5 \times 50$ mm was used, with a total number of 12,500 nodes and 85,095 lattice elements (Fig. 7). To

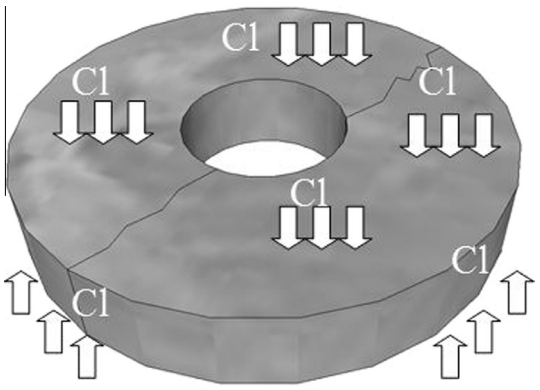

Fig. 6. Brick/mortar specimen of [26,27].

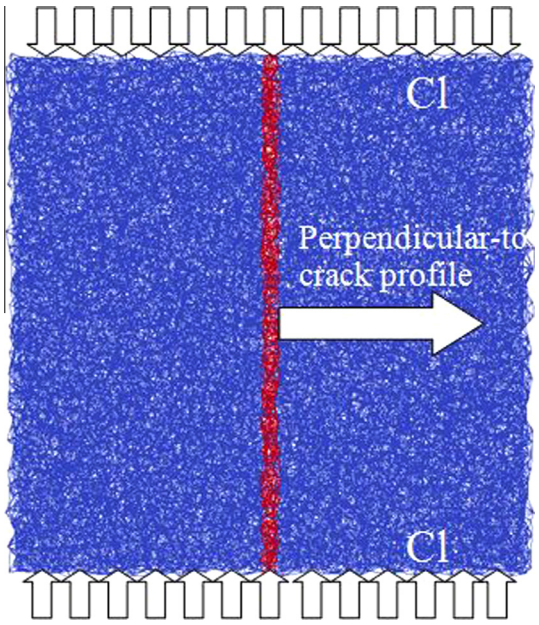

Fig. 7. Lattice used in the simulations. Blue – brick/mortar, red – "crack". (For interpretation of the references to color in this figure legend, the reader is referred to the web version of this article.)

simplify the process at this stage, the mechanical analysis is not performed here; rather an artificial "crack" is created in the middle of the analyzed specimen (red lattice elements in Fig. 7). Different transport properties of "cracked" elements (D_{CR}) are needed to reproduce experimental results for different crack widths. A trial-and-error approach was then taken: transport properties of these lattice elements (i.e. red elements in Fig. 7) were adjusted in order to obtain a good match between simulation results and experiments. The fitting procedure was performed for every crack width, providing a range of values of D_{CR} for different crack widths. The results are discussed below.

First, experimental results of cracked brick specimens are reproduced [26]. After cracking, these were fitted in the chloride penetration cell, and exposed for 10 hours. Regression analysis of the chloride profile perpendicular to the exposed surface (uncracked sample) yielded the diffusion coefficient of 156.71×10^{-12} m^2/s, and the surface chloride concentration of 0.37% per weight of sample (Fig. 8). These were used as input for all analyses of this experiment.

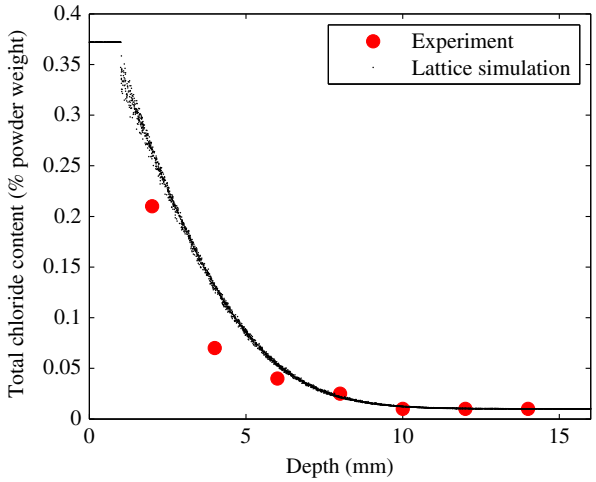

Fig. 8. Surface chloride profile-uncracked sample (brick).

In order to obtain results close to experimental values, a trial-and-error procedure was followed. This means that the effective diffusion coefficient of "cracked" elements was adjusted until the calculated perpendicular-to-crack profile corresponded well to the experimental one. Values of the fitted effective diffusion coefficients for different crack widths are shown in Fig. 9.

For large cracks (60 μm and 128 μm), the effective diffusion coefficient is 3 orders of magnitude higher than the diffusion coefficient of chloride ions in free bulk water (which is around 2.03×10^{-9} m^2/s at 20 °C [28]). An ionic diffusion coefficient this high is impossible to achieve in liquid water. However, these results seem to be in good accordance with values proposed by Wang and Ueda [7]. They also suggested that the effective diffusion coefficient in large cracks in brick samples is very high, much higher than that in free bulk water. They attributed this to additional transport mechanisms which may occur in the crack, e.g. "convection current due to the small temperature gradient and/or small hydraulic pressure gradient" [7], and further used these values to model chloride diffusion in cracked concrete. However, it seems also possible that, even though the experiment aimed at determining local diffusion coefficient of chloride ions in cracks, the brick specimens had not been completely saturated when the experiment begun. Therefore, capillary suction might have played a significant role, if by accident. Due to high porosity of brick samples, this could strongly influence the chloride ingress behavior, and explain these high diffusion coefficients. The validity of these assumptions is addressed later on. Nevertheless, based on the present tests, the following (tentative) linear relation can be proposed:

$$D_{CR} = (23.84 \cdot w + 8.37) \times 10^{-11} \quad (\mathrm{m}^2/\mathrm{s}) \text{ for } 21\ \mu\mathrm{m} \leqslant w \leqslant 55\ \mu\mathrm{m}$$
$$D_{CR} = 1.4 \times 10^{-6} \quad (\mathrm{m}^2/\mathrm{s}) \text{ for } w > 55\ \mu\mathrm{m}$$

The lower bound of 21 μm in (21) represents the smallest tested crack width [26]. When the crack is smaller than this, it can be considered that no increase in the diffusion coefficient occurs. The value of 55 μm in (21) was selected based on the recommendation of Ismail et al. [26]. It was found, after performing a deformation-controlled uniaxial tension test on the material, that the critical crack opening of about 50–55 μm is where the mechanical interaction between crack surfaces ceases to exist, so there can be no reduction of the chloride diffusion in larger cracks. This value is higher for concrete, where, due to material heterogeneity, more crack bridging and branching occurs.

In order to check whether these results are directly applicable to cement based materials, the same experiment, but this time on cracked mortar samples, was simulated [27]. In this work, two series of mortar specimens were cracked at different ages (28 days and 2 years). These were tested in order to check also the influence of cracking age on autogeneous healing of cracks. Regression analyses of perpendicular-to-surface profiles yielded the following data: diffusion coefficient of 8.66×10^{-12} m^2/s, surface chloride concentration of 0.32% mortar weight; and the diffusion coefficient of 7.51×10^{-12} m^2/s, surface chloride concentration of 0.32% mortar weight, for 28 days and 2 years series, respectively. In both instances, specimens were exposed to chloride loading for a total of 14 days.

Based on (21), effective diffusion coefficients for different crack widths were calculated. After the analyses were performed, the results indicated that (21) overestimated the perpendicular-to-crack diffusion in cracked mortar (Fig. 10). A different relation [29] was also used to check whether it gives better results when applied to cement-based materials:

$$D_{CR} = 2 \times 10^{-11} \cdot w - 4 \times 10^{-10} \quad (\mathrm{m}^2/\mathrm{s}) \text{ for } 30\ \mu\mathrm{m} \leqslant w < 80\ \mu\mathrm{m}$$
$$D_{CR} = 1.4 \times 10^{-9} \quad \mathrm{m}^2/\mathrm{s} \text{ for } w \geqslant 80\ \mu\mathrm{m}$$

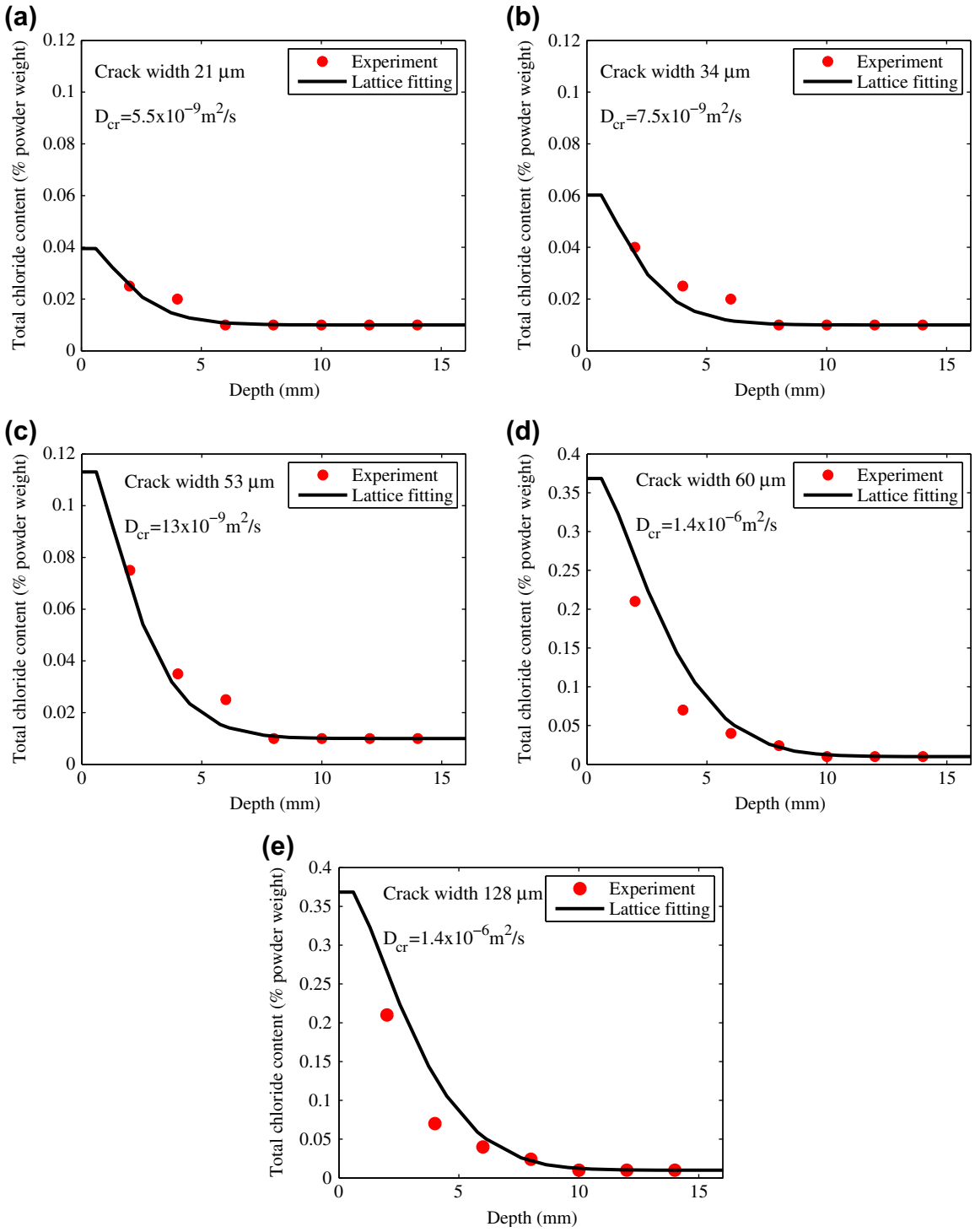

Fig. 9. (a–e) Perpendicular-to-crack chloride profiles for different crack widths (brick).

The lower bound in the Eq. (22) accounts for crack healing (30 μm). The upper bound (80 μm) is where mechanical interaction between the crack faces ceases to exist (higher for concrete than for brick-see (21)).

Comparison of the simulations performed with use of both (21) and (22) is shown in Fig. 10. Note that (22) was used here also for a crack narrower than 30 μm (29 μm in this case), which was created in mortar after 2 years. Unlike the specimens cracked at a young age, these older specimens have a diminished autogeneous healing potential. This is due to the fact that the amount of unhydrated cement is low in these samples.

Clearly, values obtained from Eq. (21) overestimate the perpendicular-to-crack chloride penetration in this case. On the contrary, results obtained using (22) are in good agreement with the experiments. It seems, then, that the values which hold for cracked brick specimens overestimate the chloride penetration in cracked mortar. Since brick is much more brittle and homogeneous, less crack branching and bridging occurs when it cracks. This potentially

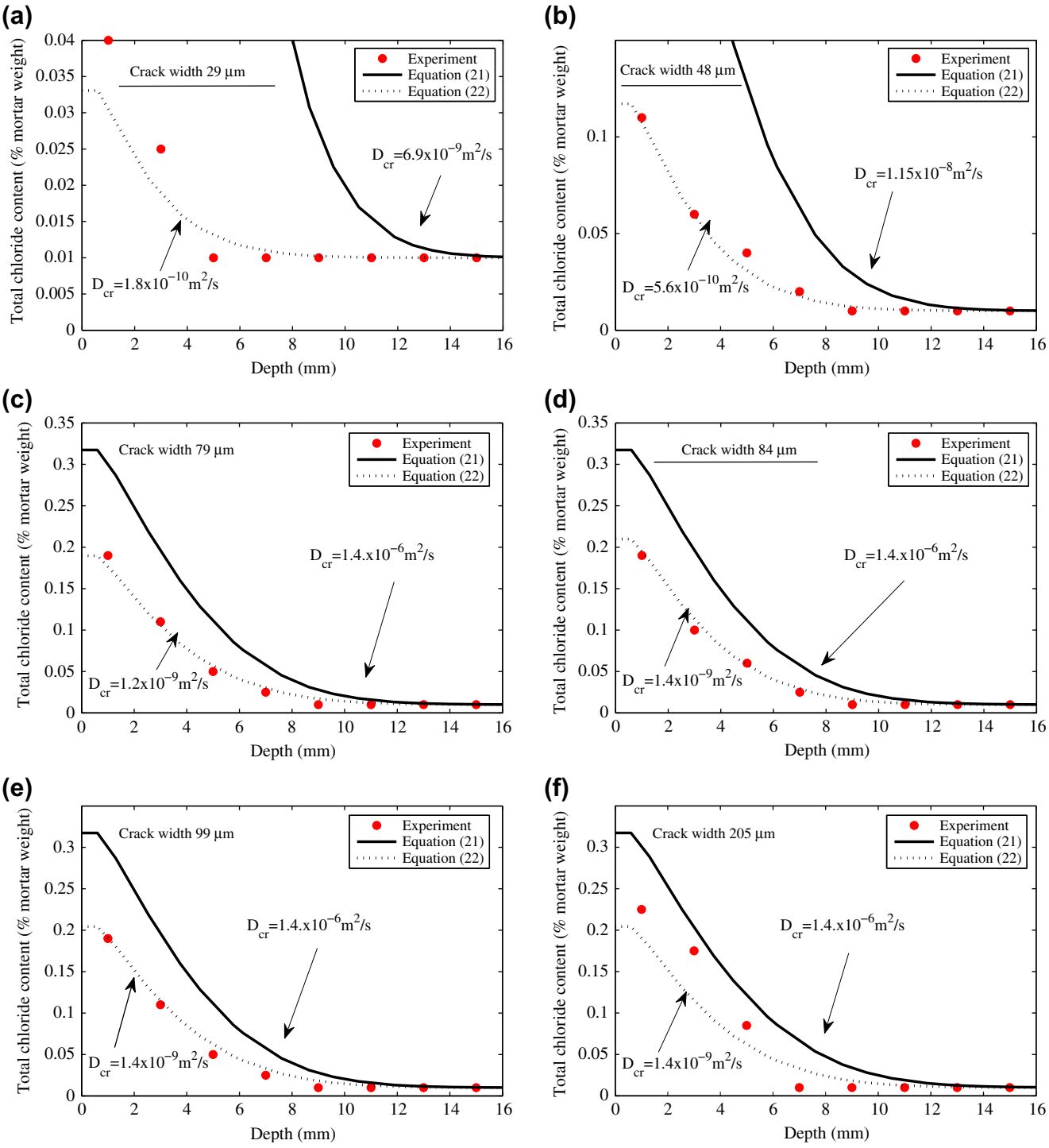

Fig. 10. (a–f) Perpendicular-to-crack chloride profiles for different crack widths (mortar). Not underlined-cracked at 28 days. Underlined-cracked at two years.

slows down chloride ingress through cracks in heterogeneous materials, like mortar and concrete. Also, it is most probable that capillary suction played a significant role in brick experiments [26], thereby altering the effective transport properties of a crack. Moreover, whether results from tests on different materials can be applied directly to mortar and concrete is questionable. In the mechanical lattice model with embedded aggregate particles, crack branches and bridges will be found automatically, and are slowing down the diffusion process. It can be, therefore, concluded that Eq. (22) can be used to simulate chloride penetration in cracked cement based materials using the proposed lattice approach.

3. Validation and discussion

3.1. Heterogeneous material

In order to validate the approach developed in Section 2.3, experimental results provided by Yang and Wang [25] were used. A 90-day ponding test was used to determine the diffusion coefficient of different concretes. All concrete mixes used in their study had a volumetric content of coarse aggregates of about 30%., with maximum grain size of 10 mm. For the simulation, a concrete material structure with about 30% of coarse aggregate particles

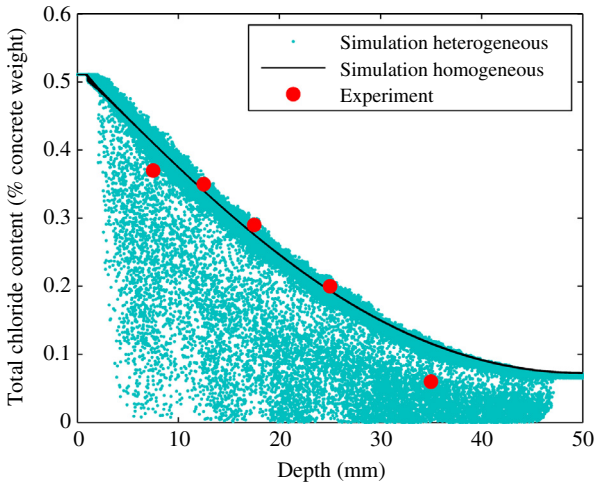

Fig. 11. Comparison of the homogeneous and heterogeneous lattice analyses and the experiment.

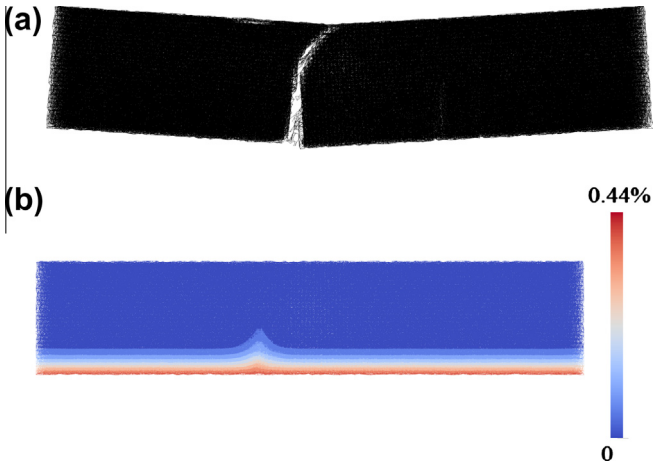

Fig. 13. (a and b) Mortar sample with surface crack width of 369 μm. Top – crack pattern (side view). Bottom – total chloride profile (% of mortar weight) after 30 days of exposure.

was generated, with coarse aggregate particle diameters ranging from 4 to 10 mm. A lattice with characteristic elements size (voxel size) of 1 mm was projected on top of it, and volume of lattice elements of each phase was calculated (61.60% mortar, 22.50% aggregate, and 15.90% interface). The total size of the mesh was $50 \times 50 \times 50$ mm, with 125,000 nodes and 938,156 lattice elements. This particular mix was made using ASTM Type I Portland cement as a binder.

Regression analysis of experimental data yielded the following: diffusion coefficient of 47.614×10^{-12} m^2/s, and surface chloride content of 0.51%. Using Eqs. (18) and (19) and the D_I/D_M value of 3, diffusion coefficients of the mortar and the interface phases were calculated as 48.35×10^{-12} m^2/s, and 145.06×10^{-12} m^2/s, respectively.

An analysis was performed using both the homogeneous and the heterogeneous lattices, using the input data as provided above. Fig. 11 shows that the results of both homogeneous and heterogeneous lattice analyses correlate well with experimentally obtained data. Zero values in the heterogeneous lattice analysis correspond to lattice nodes which are inside the impermeable aggregate particles; therefore, no chloride ions can be present. Other points below the maximum penetration band show that, in a heterogeneous material as modeled here, there is no sharp front of chloride penetration. Instead, a three-dimensional profile is present, with variable chloride content at a certain depth. It can also be seen that there exists a difference between the maximum total chloride content at a certain depth (the one obtained from the heterogeneous analysis), and the value which is obtained if concrete is considered to be a homogeneous medium. By performing similar analyses (but considering concrete as a two-phase medium, comprising mortar and coarse aggregates), this phenomenon also occurred in other studies [30,31]. They suggested that this could be one of the factors contributing to large discrepancy in values of critical chloride contents reported in the literature. It is possible that a threshold value of chloride is reached in certain points on the reinforcing steel, thus depassivating it and creating local corrosion pits. However, chloride content elsewhere along the steel could be lower, due to material inhomogeneity. Due to the usual experimental procedure (i.e. grinding the material close to the reinforcing steel and performing chemical analysis to determine the chloride content), the value obtained would be lower than the actual value which caused the local depassivation of the steel. This phenomenon justifies the use of more advanced material models, such as the presented one, in order to get more insight into the process of steel depassivation and corrosion pit locations in concrete. Also, it encourages the use of more sophisticated experimental techniques, such as laser-induced breakdown spectroscopy (LIBS) [32] or electron probe microanalysis (EPMA) [33], especially when determining the value of critical chloride content in concrete (Figs. 12 and 13).

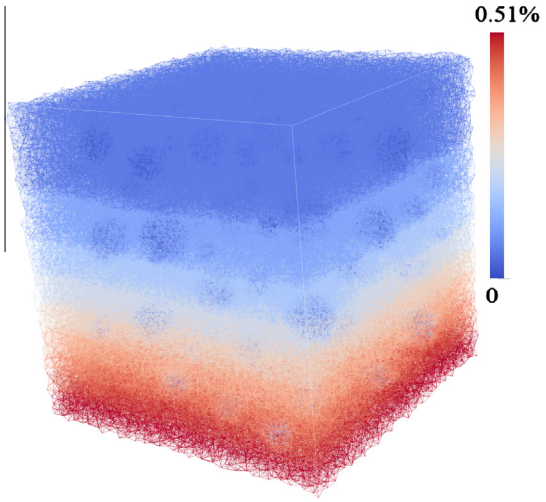

Fig. 12. Total chloride content from the heterogeneous analysis (% of concrete weight).

3.2. Cracked material

The approach presented in Section 2.4. was verified on experimental results of Şahmaran [34]. Mortar prisms ($355.6 \times 50.8 \times 76.2$ mm) reinforced with three levels of steel mesh reinforcement were cast. The prisms were reinforced to enable creation of cracks of varying controlled widths. After the curing period, they were cracked using 4-point bending test to obtain different crack widths. After loading, one single crack occurred in each of the specimens. Cracks formed in bending are tapered (V-shaped). Upon unloading, some crack closure occurred, so their width was measured in the unloaded state. Then, the samples were exposed to NaCl solution for 30 days. After the exposure period, area around the crack was drilled, ground, and analyzed for chloride.

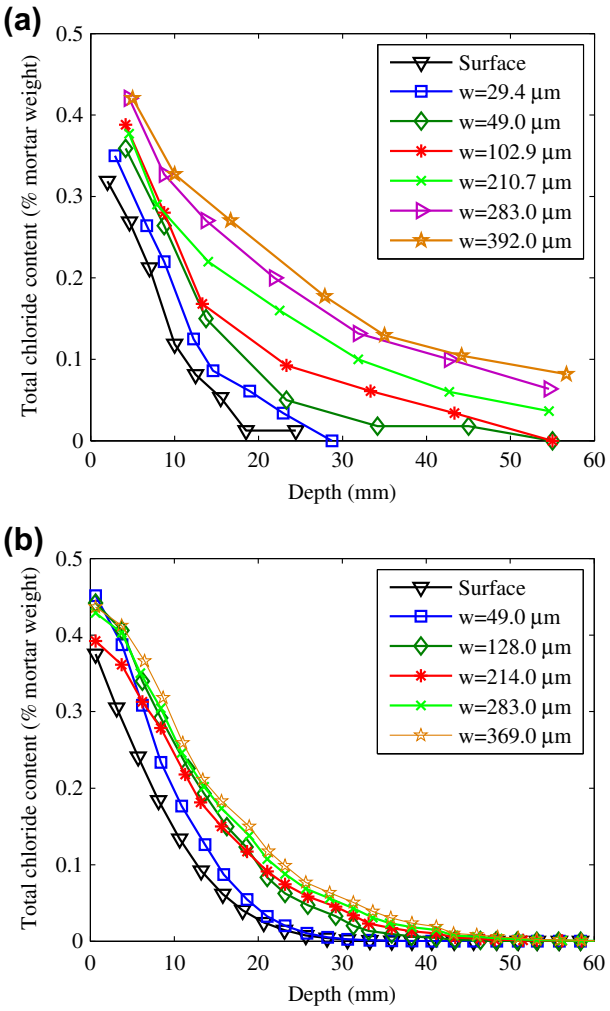

Fig. 14. (a and b) Total chloride profiles for different crack widths after 30 days of exposure. A – experiment; B – simulation.

Regression analysis of the experimental data gave the following (for the uncracked sample): diffusion coefficient of 20.3×10^{-12} m^2/s, and surface chloride content of 0.39% by weight of mortar. The analyzed sample had a size of $355 \times 50 \times 75$ mm, with a characteristic element size of 2.5 mm. Steel mesh reinforcement was neglected in the simulation. First, a mechanical analysis was performed. Using a four-point bending setup, cracks of different widths were produced. As in the experiments, one single crack formed in the fracture analysis. The output of the mechanical analysis was used as input for the chloride diffusion analysis. Eq. (22) was used for defining the effective diffusion coefficients of cracks. Every "local" cracked element has its own value of the diffusion coefficient, depending on its crack width.

Several analyses were performed using the range of surface crack widths similar to the experiments. The surface chloride contents for each analysis were adjusted to match those in experiments with a similar crack width. Both experimental and simulation results are shown in Fig. 14.

As expected, chloride penetration depth increases with the increase of surface crack width. The effect is less pronounced than in the case of a parallel-walled crack, though. This is due to the fact that bending cracks are V-shaped, being wider at the surface than on the inside of the prism. According to Eq. (22), cracks wider than 80 μm all have the same effective diffusion coefficient. However, since wider bending cracks also run deeper, the effect of widening is still pronounced with large cracks. This means that widening of the cracks above the 80 μm threshold does increase chloride penetration further, since they become deeper in the process.

Comparing the experimental and simulation results (Fig. 14), evidently there is a difference. Experimental results for wider cracks (more than 210 μm) show a more pronounced influence of cracking, compared to simulation results. There are two reasons for this: first, the crack width was measured in the unloaded state. This means that the crack was larger during the loading and some damage was created, which is not accounted for in the model. Secondly, some cracks have probably formed alongside the steel mesh reinforcement, speeding up the lateral chloride penetration. This was disregarded in the model. Overall, the simulation results seem to be in relatively good agreement with experimental data. Accordingly, the approach developed in Section 2.4 can be successfully employed in simulating chloride ingress in cement based materials cracked in flexure.

4. Summary and conclusions

As cementitious materials are highly inhomogeneous and cracked, their transport properties show significant local variations. More advanced models than presently available are needed for studying these effects. In view of this, a three-dimensional lattice model for simulating chloride ingress was developed. The proposed framework described here enables:

(1) Simulating chloride ingress in heterogeneous concrete, i.e. taking into account the presence of impermeable aggregate particles and porous interface surrounding them.
(2) Taking into account presence of cracks on chloride ingress, by coupling the simulation with the mechanical analysis.

In order to focus on these two issues, saturated concrete was assumed in all analyses.

The procedures developed were tested and validated using data from the available literature. The following conclusions can be reached from the presented numerical simulations:

(1) When neglecting the material heterogeneity, simulation results are very close to experimental ones. The reason for this lays in the usual experimental procedure (grinding and chemical titration), which gives an averaged value of the chloride content at a certain depth.
(2) The heterogeneous model shows some deviation from the perfect diffusion profile, which is commonly observed in experiments where penetration depth is determined by silver nitrate spraying. More importantly, maximum chloride contents at a certain depth are higher than the averaged ones. This should be kept in mind, especially when studying the critical chloride content in concrete. Use of more advanced experimental methods is therefore encouraged.
(3) Mechanical cracks do promote chloride ingress into concrete, depending on their width. This is observed also in the model. However, even though commonly addressed only by their surface widths, not all cracks are created equal. Bending cracks are V-shaped, meaning that a part of the crack close to its tip remains inaccessible for rapid chloride penetration. Thus, parallel walled cracks of a certain surface width are more detrimental than flexural cracks of the same surface crack width. Coupling of the mechanical and transport model, as proposed here, enables studying this behavior in more detail.

In all the analyses presented here, it was assumed that concrete was fully saturated. Consequently, capillary suction was not considered. Also, effects of chloride binding have not been explicitly taken into account [35], and no distinction was made between free and bound chloride ions. Rather, the effective diffusion coefficient of the material was used in the simulations. For the laboratory experiments simulated, performed in controlled conditions and short term, these are valid assumptions. However, for engineering service-life analyses, these effects should not be neglected.

Finally, it can be concluded that the presented model can be successfully employed in simulating chloride penetration in both sound and cracked cement based materials. Presence of coarse aggregates in concrete can be included in the model, and gives more insight on the transport behavior.

Acknowledgements

Financial support by the Dutch Technology Foundation (STW) for the project 10978 – "Measuring, Modelling, and Monitoring Chloride ingress and Corrosion initiation in Cracked Concrete (M3C4)" is gratefully acknowledged. Constructive comments and suggestions of the reviewers are appreciated.

References

[1] Šavija B, Schlangen E. Chloride ingress in cracked concrete – a literature review. In: Andrade C, Gulikers J, editors. Advances in modeling concrete service life. Springer; 2012. p. 133–42.
[2] Pacheco J, Polder RB. Corrosion initiation and propagation in cracked concrete – a literature review. In: Andrade C, Gulikers J, editors. Advances in modeling concrete service life. Springer; 2012. p. 55–93.
[3] Rahman MK, Al-Kutti WA, Shazali MA, Baluch MH. Simulation of chloride migration in compression-induced damage in concrete. J Mater Civil Eng 2012;24(7):789–96.
[4] Boulfiza M, Sakai K, Banthia N, Yoshida H. Prediction of chloride ions ingress in uncracked and cracked concrete. ACI Mater J 2003;100(1):38–48.
[5] Adiyastuti SM. Influence of cracks on chloride induced corrosion in reinforced concrete structural members. PhD Thesis. Sydney: University of New South Wales; 2005.
[6] Ožbolt J, Balabanić G, Periškić G, Kušter M. Modelling the effect of damage on transport processes in concrete. Constr Build Mater 2010;24:1638–48.
[7] Wang L, Ueda T. Mesoscale modelling of the chloride diffusion in cracks and cracked concrete. J Adv Concr Technol 2011;9(3):241–9.
[8] Poulsen E, Mejlbro L. Diffusion of chloride in concrete: theory and application. New York (USA): Taylor & Francis; 2006.
[9] Schlangen E. Experimental and numerical analysis of fracture processes in concrete. PhD Thesis. Delft: Delft University of Technology; 1993.
[10] Sadouki H, van Mier JGM. Meso-level analysis of moisture flow using a lattice-type approach. Mater Struct 1997;30:579–87.
[11] Bolander JE, Berton S. Simulation of shrinkage induced cracking in cement composite overlays. Cem Concr Comp 2004;26:861–71.
[12] Grassl P. A lattice approach to model flow in cracked concrete. Cement Concrete Comp 2009;31(7):454–60.
[13] Grassl P, Fahy C, Gallipoli D, Bolander JE. A lattice model for fracture and mass transport in concrete. In: Ye AA et al., editors. Second international conference on microstructural related durability of Cementitious Composites, April 11-13, 2012, Amsterdam, the Netherlands.
[14] Nakamura H, Srisoros W, Yashiro R, Kunieda M. Time-dependent structural analysis considering mass transfer to evaluate deterioration process of RC structures. J Adv Concr Technol 2006;4(1):147–58.
[15] Yip M, Mohle J, Bolander JE. Automated modeling of three-dimensional structural components using irregular lattices. Comput-Aid Civ Infrastruct Eng 2005;20:393–407.
[16] Qian Z. Multiscale modeling of fracture processes in cementitious materials. PhD Thesis. Delft: Delft University of Technology; 2012.
[17] Schlangen E, Qian Z. 3D modeling of fracture in cement-based materials. J Multiscale Modell 2009;1(2):245–61.
[18] Landis E, Bolander JE. Understanding material behaviour by integrating numerical simulation with 3D microstructural imaging. In: Leung CKY, Wan KT, editors. International conference on advances in construction materials through science and engineering, Hong Kong; 2011.
[19] Delagrave A, Bigas JP, Ollivier JP, Marchand J, Pigeon M. Influence of the interfacial zone on the chloride diffusivity of mortars. Adv Cem Based Mater 1997;5(3–4):86–92.
[20] Schlangen E, Garboczi EJ. Fracture simulations of concrete using lattice models: computational aspects. Eng Fract Mech 1997;57(2/3):319–32.
[21] Lewis RW, Nithiarasu P, Seetharamu KN. Fundamentals of the finite element method for heat and fluid flow. New York: John Wiley & Sons; 2004.
[22] Caré S, Hervé E. Application of a *n*-phase model to the diffusion coefficient of chloride in mortar. Transport Porous Med 2004;56(2):119–35.
[23] Oh BJ, Jang SY. Prediction of diffusivity of concrete based on simple analytic equations. Cem Concr Res 2004;34:463–80.
[24] Tang L et al. Guideline for practical use of methods for testing the resistance of concrete to chloride ingress. EU-Project CHLORTEST. Project No: G6RD-CT-2002-00855; 2005.
[25] Yang CC, Wang LC. The diffusion characteristic of concrete with mineral admixtures between salt ponding test and accelerated chloride migration test. Mater Chem Phys 2004;85:266–72.
[26] Ismail M, Toumi A, François R, Gagne R. Effect of crack opening on the local diffusion of chloride in inert materials. Cem Concr Res 2004;34:711–6.
[27] Ismail M, Toumi A, François R, Gagne R. Effect of crack opening on the local diffusion of chloride in cracked mortar samples. Cem Concr Res 2008;38:1106–11.
[28] Hill D. Diffusion coefficients of nitrate, chloride, sulphate and water in cracked and uncracked Chalk. J Soil Sci 1984;35(1):27–33.
[29] Djerbi A, Bonnet S, Khelidj A, Baroghel-Bouny V. Influence of traversing crack on chloride diffusion into concrete. Cem Concr Res 2008;38:877–83.
[30] Yu H, Hartt WH. Modeling corrosion initiation of reinforcing steel in concrete: effect of non-diffusive coarse aggregate. J Compos Mater 2011;45(2):153–69.
[31] Soive A, Baroghel-Bouny V. Influence of gravel distribution on the variability of chloride penetration front in saturated uncracked concrete. Constr Build Mater 2012;34:63–9.
[32] Weritz F, Schaurich D, Taffe A, Wilsch G. Effect of heterogeneity on the quantitative determination of trace elements in concrete. Anal Bioanal Chem 2004;385(2):248–55.
[33] Win PP, Watanabe M, Machida A. Penetration profile of chloride ion in cracked reinforced concrete. Cem Concr Res 2004;34:1073–9.
[34] Şahmaran M. Effect of flexure induced transverse crack and self-healing on chloride diffusivity of reinforced mortar. J Mater Sci 2007;42:9131–6.
[35] Martín-Peréz B, Zibara H, Hooton RD, Thomas MDA. A study of the effect of chloride binding on service life predictions. Cem Concr Res 2000;30:1215–23.